Cleaner Engineering and Technology 23 (2024) 100839

Contents lists available at ScienceDirect

Cleaner Engineering and Technology

journal homepage: www.sciencedirect.com/journal/cleaner-engineering-and-technology

# Spent coffee ground biochar for phosphate adsorption in water: Influence of pyrolysis temperature and iron-coating activation method

Alessia Torboli [a,*], Paola Foladori [a], Mingming Lu [b], Stefano Gialanella [c], Lorena Maines [c]

[a] Department of Civil, Environmental and Mechanical Engineering, University of Trento, via Mesiano 77, 38123, Trento, Italy
[b] College of Engineering and Applied Science, University of Cincinnati, 2901 Woodside Drive, Cincinnati, OH, 45221, United States
[c] Department of Industrial Engineering, University of Trento, via Sommarive 9, 38123, Trento, Italy

ARTICLE INFO

*Keywords:*
Biochar
Iron-coated biomass
Phosphate adsorption
Spent coffee grounds
Waste upcycle
Water purification

ABSTRACT

A substantial portion of the phosphorus utilized in crop and food production is dispersed into soil and water, posing a challenge to the management of eutrophication and sustainable nutrient recovery. This research focuses on the reclamation of phosphate from polluted water through affinitive adsorption on biochar derived from spent coffee grounds (SCG). SCG were subjected to pyrolysis within a $N_2$-purged vertical furnace across a temperature range of 300–550 °C, with a 1-h holding time. The adsorption capability of SCG biochar was systematically investigated and experimental data were interpreted using Langmuir and Freundlich isotherm models. Notably, the biochar pyrolyzed at 450 °C and activated with a Fe/biochar mass ratio of 2:1 demonstrated the highest adsorption capacity (0.87 mg P/g biochar) when exposed to the highest initial phosphate concentration in the solution (15 mg P/L). Comparative analyses revealed that the removal efficiency of non-activated SCG biochar was considerably lower (5.7%) compared to the corresponding activated biochar (up to 17.3%). This highlights the significant increase in adsorption capacity facilitated by the introduction of ferric chloride. Furthermore, phosphate desorption experiments were conducted to assess the biochar's phosphorus release characteristics and stability. The results demonstrate the positive outcomes of upcycling SCG waste material as a pollutant sorbent and the potential to diminish reliance on chemical fertilizers through the recovery of Fe-phosphate-enriched SCG biochar.

## 1. Introduction

Phosphorus (P) is a non-replaceable nutrient for the growth of all living organisms and essential for agricultural productivity, guaranteeing food security to the growing world's population (Schröder et al., 2010). Every year, the world population generates, from the food consumed, about 3 million tons of phosphorus in urine and feces (Cordell et al., 2012) with an average of 0.5 kg P per person per year, that is in large part discharged in water and non-agricultural land, worsening the phenomena of eutrophication in aquatic systems. Human consumption in food represents only 20% of the total P extracted from the geological and not renewable reserves of phosphate rocks, the remainder is used for the production of fertilizers, zootechnical foods, pesticides, detergents (Cordell et al., 2012). Various estimates indicate that, at the current rate of extraction, phosphorus will prove to be a limited resource within 50–100 years, with costs destined to increase more and more (Cordell et al., 2012). Given the environmental and economic relevance of the matter, strategies that simultaneously protect the aquatic ecosystem from eutrophication, diminish the dependence on mineral phosphate rocks and support agricultural and food system productivity are mandatory.

Similarly to activated carbon, biochar is a carbon-rich material manufactured through the thermochemical conversion of carbonaceous material at temperature above 300 °C under negligible oxygen supply but over a significantly shorter period of time, 2 h and below.

To create an oxygen-depleted atmosphere within the reactor, the pyrolysis process is optimally performed under inert conditions, using a fluidizing gas such as nitrogen. While other inert gas like helium, and non-inert gases such as $CO_2$, $H_2$, and $NH_2$ have been employed during pyrolysis, nitrogen is the most used gas due to its inert nature, cost-effectiveness compared to other inert gases, and ready availability (Sharma et al., 2024).

Biochar possesses highly desirable properties including a large surface area, porous structure, ion exchange capacity, and substantial

* Corresponding author.
*E-mail address:* alessia.torboli@unitn.it (A. Torboli).

https://doi.org/10.1016/j.clet.2024.100839
Received 12 December 2023; Received in revised form 7 August 2024; Accepted 13 November 2024
Available online 15 November 2024

carbon content (Ahmad et al., 2014). These properties enable it to efficiently adsorb a wide range of contaminants from aqueous solutions. Furthermore, the surface of biochar is comprised of a certain number of functional groups, such as hydroxyl, carboxyl, and carbonyl (Chen et al., 2008), which can be activated to be highly selective towards specific pollutants targets (Lu et al., 2020). For example, biochar can be functionalized to accommodate iron salts, enhancing its affinity towards phosphates. (Li et al., 2014). Through the formation of phosphate-iron complexes, phosphate can potentially be reclaimed from wastewater via affinitive adsorption. The resultant biochar, enriched with Fe-phosphate, can be recovered, and potentially reused for soil remediation (Sheperd et al., 2016). In addition, the costs of raw materials for biochar production are extremely lower than that of activated carbon since it may derive from waste feedstocks, such as wood chips, agricultural and sewage wastes.

At present, although the production process of biochar is robust and simple, the knowledge about adsorption and desorption properties of this material is in the early stages and further research is required, especially in view of future large-scale development. Indeed, although biochar exhibits similar properties as activated carbon, its heterogeneity leads to many uncertainties when applied in engineered plants (Gwenzi et al., 2017). Additionally, different feedstocks yield varying ratios of volatile and stabilized carbon in pyrolysis by-products, significantly influencing the morphological and physicochemical properties of the resulting biochar (Sahoo et al., 2021). Feedstoc-related properties that influence phosphate adsorption capacity include biochar's surface area, porosity, surface functional groups, and mineral content (Luo et al., 2023). Feedstocks that can withstand higher pyrolysis temperatures typically lead to biochar with increased surface area and porosity (Tomczyk et al., 2020), though this can also diminish the number of surface functional groups (Trazzi et al., 2016). Conversely, feedstocks rich in organic matter and nutrients produce biochar with a greater abundance of surface functional groups, such as carboxyl, hydroxyl, and phenolic groups (Rizwan et al., 2023). These functional groups enhance phosphate adsorption by forming bonds with phosphate ions (Luo et al., 2023). Additionally, feedstocks with high mineral content, like animal manure or specific agricultural residues, produce biochar that facilitates the precipitation of phosphate as insoluble compounds, thereby enhancing its adsorption capacity (Luo et al., 2023). High ash content in biochar can also increase its pH and create additional adsorption sites through the presence of metal oxides and hydroxides in the ash (Guo et al., 2020).

Feedstocks currently used at a commercial-scale or in research facilities for the removal of phosphate from water and wastewater are mainly agricultural residues, food processing waste, municipal solid waste, and sludge. Raw materials include walnut shell and sewage sludge (Yin et al., 2019), coconut shell (Kopecký et al., 2020), wood and rice husks (Ajmal et al., 2020), and pig manure (Nardis et al., 2022). Careful selection of feedstocks, production parameters and modification methods is critical for optimizing biochar production and its specific applications.

This paper focuses on a promising waste material, spent coffee ground, for the production of biochar and its application as base sorbent for phosphate remediation from aqueous solution, in order to evaluate the potential application to wastewater. Coffee is the world's second most consumed beverage next to water, with a consumption in 2021 of approximately 10 million tons (Johnson et al., 2022) but SCGs are mainly disposed of as waste in landfill. SCGs can be obtained in higher purity than other waste materials and SCG biochar has been functionalized for removing various pollutants. For these reasons, biochar produced from spent coffee grounds is viewed as a low-cost and environmentally friendly substitute for activated carbon. Utilizing SCG biochar for phosphate removal and recovery presents several simultaneous advantages, including the exploitation of a waste product to avoid disposal in unsustainable destinations, enrichment of this adsorbent with phosphates removed from polluted water, and availability of a phosphate-rich substrate as a sustainable alternative to chemical fertilizers.

The present research aims to advance our understanding of the SCGs biochar manufacturing process and activation treatments. The characteristics of the feedstock, such as its chemical composition, moisture content, and mineral content, may differ from that of biochar produced from other biomasses, which may lead to variations in the properties of the resulting biochar (Ahmed et al., 2024). Specifically, the research focuses on: (i) the impact of pyrolysis temperature on key SCG-derived biochar properties such as production yield, elemental composition, morphology, and functional groups, (ii) the efficacy of iron-coating activation treatment, (iii) the enhancement of adsorption capacity through temperature variation and activation treatment.

By providing a comprehensive analysis of biochar properties and its applications in phosphate recovery, this study serves as an additional contribution to the development of environmentally sustainable biochar-based materials aimed at promoting a circular economy.

## 2. Materials and methods

### 2.1. Biochar production and characterization

Moisture-laden coffee waste taken from Starbucks Coffee Shop was dried at 50 °C for 48 h to remove moisture and subsequently used as initial feedstock for biochar production. For the pyrolysis treatment, dried spent coffee grounds (SCGs) were placed in a quartz tube and heated in a vertical furnace, programmed to hold a desired temperature for a desired time, in the presence of nitrogen gas ($N_2$). A temperature automation device (*Automation Direct Solo 4848 Temperature Controller*) was connected to the furnace heating system and encoded to provide ramp temperature, set by entering initial temperature, final temperature, and time elapsed between the two values. In detail, the automation device provided a ramp temperature of 5 °C/min in the first ramping phase and a constant temperature in the second stage. SCGs were burnt for a holding time of 1 h and then the reactor was set to cool down to room temperature. A set of 5 different temperatures between 300 and 550 °C were applied and the manufactured biochar is hereinafter referred to as 300 °C $N_2$, 350 °C $N_2$, 450 °C $N_2$, 500 °C $N_2$, 550 °C $N_2$ SCG biochar to differentiate it from unheated SCG. After pyrolysis treatment, biochar was washed by organic solvent (dichloromethane, DCM) to remove polycyclic aromatic hydrocarbons (PAHs), and by distilled water (DW). Indeed, incomplete combustion or pyrolysis of organic materials leads to PAH formation (Wang et al., 2017). Nguyen et al. (2019) elucidated that the formation of PAHs during the pyrolysis of spent coffee ground occurs via direct temperature-induced dehydration, decarboxylation, and dehydrogenation reactions, leaving behind aromatic rings. Biochar pyrolyzed at high temperature results in the loss of C, H, O and N content, leading to a higher yield of multi-aromatic ring PAHs. Although the total PAH concentrations of SCG biochar in Nguyen et al. (2019) study were found to be lower than safe threshold values for biochar as required by the International Biochar Initiative, a simplified and rapid solvent extraction with dichloromethane was applied to eliminate health risks of PAHs.

Production yield of biochar, starting from raw SCG, was assessed by measuring the weight before and after they have been pyrolyzed.

Values of pH were measured on wastewater collected in mason jars during pyrolysis and during wash procedure with DCM (dichloromethane) and DW (deionized water). The final pH of the biochar surface is thus given by the pH of wash water.

Elemental (C, H, N) analysis was performed with an elemental analyzer (LECO mod. CHN628 Carbon/Hydrogen/Nitrogen Determinator). The levels of carbon (C), hydrogen (H), and nitrogen (N) in the manufactured biochar were measured as uniform compounds generated upon sample combustion. To measure element ratios, a carrier gas is used to facilitate the separation of the combustion gas into distinct infrared cells dedicated to detecting $H_2O$ and CO, while a thermal

conductivity cell is employed for the precise detection of nitrogen.

The morphology and microstructure of biochar were analyzed using a scanning electron microscope (SEM, mod. JEOL JSM-IT300LV). Surface element analysis of biochar was performed simultaneously through energy-dispersive X-ray spectroscopy (EDXS), employing the Bruker Quantax spectrometer coupled with the SEM.

Lastly, Fourier Transform InfraRed (FTIR) spectroscopy analysis was conducted to assess the functional groups present on the biochar surface and responsible for the adsorption of certain ions. Infra-red spectra of the biomass materials in the 4000 cm-1 and 400 cm-1 spectral range were collected with Thermo Fisher Scientific Nicolet 6700 FTIR Spectrophotometer.

### 2.2. Biochar activation

Biochar was functionalized with ferric chloride ($FeCl_3$) to enhance its selectivity toward phosphorus. Iron (hydr)oxides present a high affinity with oxy-anions such as phosphate (Li et al., 2014), suggesting that the main active sites for phosphorus adsorption can be provided by the iron coated onto the adsorbent. The activated Fe-biochar underwent a 2-h chemical impregnation in a mixed solution containing $FeCl_3$ at three different mass ratios of iron to biochar. In detail, 2 g of pyrolyzed biochar samples at each temperature range were coated with 17.9 mL, 53.7 mL, 71.5 mL volumes of 1 M $FeCl_3$, corresponding to a mass ratio of iron to biochar of 0.5, 1 and 2, respectively. The mixed solution was left to stand for 2 h at room temperature. The biochar was then filtered with a stainless-steel filter and washed with DW until pH 7 in the washing water was reached. Some biochar samples did not undergo chemical impregnation with $FeCl_3$ to assess the sorption capacity of non-activated biochar in comparison with Fe-biochar. Fe-biochar is hereinafter referred to as: 0.5:1, 1:1, 2:1 SCG biochar to differentiate it from non-activated (NA) SCG biochar.

### 2.3. Adsorption batch tests

Batch tests were carried out to determine the phosphate adsorption capacity of the adsorbent. In each test, a fixed amount of biochar (0.2 g) was added to 100 mL of phosphate solution of known concentration in 200 mL glass beakers. Phosphate solution was prepared by diluting a stock solution of $KH_2PO_4$ (1.0 g P/L) with DW to achieve the desired initial concentration.

To facilitate contact between the entire adsorbent surface area and the target pollutant, meticulous attention was given to various variables in the experimental setup, including vessel shape, contact time, stirring velocity, and adsorbent dose. In particular: (i) the beakers were stirred at a constant rate (300 rpm) for 4 h, in order to provide sufficient contact time between adsorbent and adsorbate; (ii) beakers had consistent dimensions in terms of diameter, shape, and volume, with no internal irregularities; (iii) circular cross-section reaction vessels were employed to ensure a uniform distribution of gradient velocity (Pivokonský et al., 2022); (iv) horizontal and circular stirring motions, centrally executed within the beakers, were employed to ensure adequate interaction between the adsorbent and the target pollutant over the course of the experiments.

Biochar in the suspensions was separated from the mixed liquor using a cellulose membrane filter. The pH of the mixed liquor obtained from the combination of biochar, DW and phosphate solution was measured as approximately 6.6. For optimal phosphate adsorption onto chloride ferric hydroxide precipitates, a pH between 5 and 8 is recommended, as the solubility of $FePO_4$ is minimum at pH equal to 5 (Nassef, 2012). Phosphate adsorption capacity significantly decreases at high pH values because OH- ions competes with $PO_4^{3-}$ ions, reducing the available adsorption sites for phosphate species on the adsorbent.

Tests were performed at room temperature to represent environmentally relevant conditions. The applied dose of biochar in this study, 2.0 g/L constant in all runs, was selected according to Luo et al. (2023), who investigated phosphate sorption by biochar-based adsorbents from various precursors and indicated typical biochar dosages from 1.0 g/L to 10 g/L.

Initial P concentration was set at concentrations around typical values found in municipal wastewater (15 mg P/L). Initial and final P concentrations were analytically determined according to *Method 4110 Phosphorus* (IRSA-CNR - 29/2003) which refers to *Standard Methods: 4500-P E: Phosphorus by Ascorbic Acid*. The method is a colorimetric analysis based upon the reduction of phosphomolybdic acid to blue molybdic oxide, followed by spectrophotometric quantification.

All the experiments were carried out in duplicate and the average result was used for further calculation.

In each test, the amount of P adsorbed per biochar mass unit at the equilibrium [$q_e$, mg P/g] was calculated as:

$$q_e = \frac{C_0 - C_e}{V \cdot m}$$

where $C_0$ and $C_e$ [mg/L] are the concentrations of P in solution at the beginning of the test and at equilibrium of the adsorbate in the solution, respectively. V [L] is the volume of the batch test (constant) and m [g] is the mass of the adsorbent used. P removal efficiency [RE, %] was calculated as follows:

$$RE = \frac{C_0 - C_e}{C_0} \cdot 100$$

### 2.4. Adsorption isotherms

To compute adsorption isotherms, various adsorption tests were conducted with varying initial P concentrations ($C_0$), while employing a consistent mass (m) of biochar type that exhibited the highest adsorption capability ($q_e$) based on the combination of temperature and activation conditions (refer to section 3.4). Both Langmuir and Freundlich isotherm models were applied to interpret the experimental results.

The Langmuir adsorption model is based on the following assumptions: (i) uniform sorbent surface, meaning that each site of adsorption is equivalent; (ii) no interaction between adjacent adsorbed molecules; (iii) reversible adsorption and monolayer adsorption surface. The non-linear equation of the Langmuir isotherm is the following:

$$q_e = \frac{q_0 \, b \, C_e}{1 + b \, C_e}$$

where b [L/mg] and $q_0$ [mg/g] are the characteristics of the Langmuir equation and are the adsorption equilibrium constant, related to the binding strength of the adsorbate, and the theoretical monolayer saturation capacity, respectively. These parameters can be calculated by transforming them into their linear forms:

$$\frac{C_e}{q_e} = \frac{1}{b \, q_0} + \frac{C_e}{q_0}$$

Langmuir isotherm can also be expressed in terms of a dimensionless equilibrium parameter, $R_L$, defined by:

$$R_L = \frac{1}{1 + b \, C_0}$$

Positive adsorption is demonstrated to occur when the mean value of $R_L$ for each different initial concentration is between 0 and 1 (Tan et al., 2007).

The Freundlich model is an empirical model, usually implemented to assess the chemisorption on a heterogeneous surface. That is, the Freundlich isotherm assumes a heterogeneous surface with a non-uniform distribution of active sites and their energies over the surface. The non-linear form of the Freundlich adsorption model is given by:

$$q_e = K_f \, C_e^{\frac{1}{n}}$$

where $K_f$ [mg/g] is the Freundlich adsorption constant that represents the adsorption capacity, whereas n is an empirical parameter related to the intensity of sorption, which varies with the heterogeneity of the material. Higher values of $K_f$ indicate higher affinity towards the adsorbate, while adsorption is considered favorable when values of the empirical parameter 1/n are between 0.1 and 1 (Park et al., 2015). A good fit of the Freundlich model indicates that the adsorption of the adsorbate is mainly controlled by chemisorption and multiple processes (Fang et al., 2015). The above equation can be linearized to calculate the parameters of the isothermal model $K_f$ and n:

$$log\ q_e = log\ K_f + \frac{1}{n} log\ C_e$$

### 2.5. P desorption from biochar

To investigate the P release characteristics of biochar, phosphate desorption experiments were performed. A mass of 0.2 g P-adsorbed biochar, produced at various pyrolysis temperatures, was placed in a 100 mL beaker with 50 mL of distilled water. The beakers were continuously stirred at 500 rpm on a magnetic stirrer for 2 h at room temperature. The mixed liquor was then allowed to settle for an additional 2 h before filtration. A set of control desorption tests were conducted to verify the absence of phosphorus contamination in the work environment, or the water utilized in the experiments., which would have otherwise biased the desorption results. Furthermore, desorption experiments were performed using biochar that had not undergone prior adsorption experiments to examine P release from the raw biomass, considering phosphorus it's one of its constituents.

## 3. Results and discussion

### 3.1. Characterization of SCG biochar and influence of pyrolysis temperature

Pyrolysis temperature plays a significant role in biochar production and the consequent properties of the manufactured material. Here, temperatures of 300 °C, 350 °C, 450 °C, 500 °C, and 550 °C were applied and the properties of the different types of biochar were analyzed, considering production yield, pH, elemental analysis (C, H, N), SEM, EDXS and FTIR spectra.

Regarding pyrolysis production yield, SCG yielded a higher quantity of biochar at a lower temperature (300 °C), achieving a production yield of around 60%. However, a sharp decrease occurred at 400 °C and beyond, attributed to the release of volatile matter and non-condensable gases, resulting in a reduced production yield ranging from 25% to 30%.

The pH of biochar increased as the pyrolysis temperature increased, ranging from 3.6 at 300 °C to 5.2 at 550 °C. Notably, despite the acidic nature of the wastewater collected during the heating process prior to washing, a significant rise was observed after the dichloromethane (DCM) and distilled water (DW) wash, reaching the range of 7.1–9.8, consistently with findings from various other studies involving biomass-based biochar.

Elemental (C, H, N) analysis, employed to assess the purity and chemical composition of biochar, revealed carbon as the predominant element in biomass, constituting over 72%–82%, with variations depending on the biochar production temperature (Table 1). As expected, an increase in pyrolysis temperature resulted in higher carbon content.

Table 1 displays the H/C atomic ratio of different biochar, which varied from 1.022 to 0.546 as the pyrolysis temperature increased from 300 to 500 °C (under $N_2$ atmosphere). The decrease in the H/C atomic ratio with increasing heating temperature demonstrates that biochar is highly carbonized and exhibits higher aromaticity (Park et al., 2015). H/C atomic ratio serves as a suitable indicator for the heightened hydrophobicity and aromaticity of biochar, as well as for assessing the size of aromatic clusters and the adsorption capacity (Ahmad et al., 2014; Xiao et al., 2016). Xiao et al. (2016) elucidated that a decreased H/C atomic ratio corresponds to a heightened aromatic skeleton structure of biochar, aligning with the rectangle-like polycyclic aromatic ring model proposed in their research. Additionally, H/C atomic ratio is a relatively accurate and stable parameter compared to other atomic ratios, such as the O/C value, which reflects various reactions occurring during the biochar ageing process, namely oxidation and reduction (Xiao et al., 2016).

**Table 1**
Mass of C and H elements and H/C atomic ratio in biochar produced at 300 °C, 450 °C, 500 °C (in presence of $N_2$).

| Type of biochar | Mass [mg] | C mass [mg] | C [No. atoms] | H mass [mg] | H [No. atoms] | H/C atomic ratio [-] |
|---|---|---|---|---|---|---|
| *300°C $N_2$* | 103 | 71.79 | 3.586E+24 | 6.15 | 3.664E+24 | 1.022 |
| *450°C $N_2$* | 100 | 74.28 | 3.711E+24 | 3.86 | 2.301E+24 | 0.620 |
| *500°C $N_2$* | 103 | 82.21 | 4.107E+24 | 3.76 | 2.241E+24 | 0.546 |

Hydrogen and nitrogen are present in the biomass in significantly smaller proportions, accounting for approximately 5% and 3%, respectively. The decline in hydrogen, from 6.15% at 300 °C to 3.8–3.9% at temperatures exceeding 450 °C, can be attributed to the gradual fragmentation of the H-bonding network in lignocellulose as the heating temperature surpasses 400 °C and subsequent oxidation of the hydroxyl groups to carboxyl (Harvey et al., 2012). The residual percentage is ascribable to ash content.

Fig. 1 shows the FTIR spectra of unheated SCG compared with the manufactured biochar type 300 °C $N_2$ and 450 °C $N_2$. All biochar spectra showed peaks in the wave number range of 2800–3000 $cm^{-1}$, indicating the presence of the C-$H_n$ functional group. However, only unheated SGC and biochar 300 °C $N_2$ showed broad peaks around 3362-3375 $cm^{-1}$, attributed to the stretching vibration of the hydroxyl group. This may be linked to the presence of lignin, cellulose, and hemicellulose in the raw SGC biomass. These constituents undergo degradation and decomposition during the pyrolysis process, leading to a reduction in functional groups. Consequently, this confirms the observed sharp decline in hydrogen content in biochar pyrolyzed at temperatures exceeding 450 °C. As the pyrolysis temperature rises, the total number of functional groups decrease, in accordance with what previous studies elucidated (Trazzi et al., 2016). Biochar subjected to heat treatment displayed medium peaks in the band range of 1580–1600 and 700-800 $cm^{-1}$ (Fig. 1), possibly due to C=C stretching of cyclic alkene and bending of alkene, respectively. High-temperature (450 °C $N_2$) biochar spectra displayed a broad peak at the wave range of 1292 $cm^{-1}$, attributed to C-O stretching of aromatic ester.

EDXS analysis of unheated SCG discloses oxygen as a predominant element (Table 2). Element contents by mass percent are given as an average value of five or more EDXS analysis samples along with corresponding standard deviation (σ). A greater standard deviation variability entails that a specific element is distributed onto the biochar surface in a non-homogeneous way. Minerals, which are fundamental constituents of coffee, or coffee plant, are present in the SCG chemical composition, namely magnesium, phosphorus, potassium, and calcium, confirming the mineral characterization of spent coffee grounds referred to by De Bomfim et al. (2023). Sulphur was also found in the EDS spectra of unheated SCG, resulting from the amino acids in the coffee proteins and numerous sulphur-containing compounds, mainly volatile, that play an important role for the aroma and flavor of commercialized coffee (Lichtenberg et al., 2007).

As compared in the secondary electron detector (SED) images shown in Fig. 2, the surface of SCG appears coarse and homogeneous (Fig. 2A and B), while biochar produced from SCG presents a sponge-like

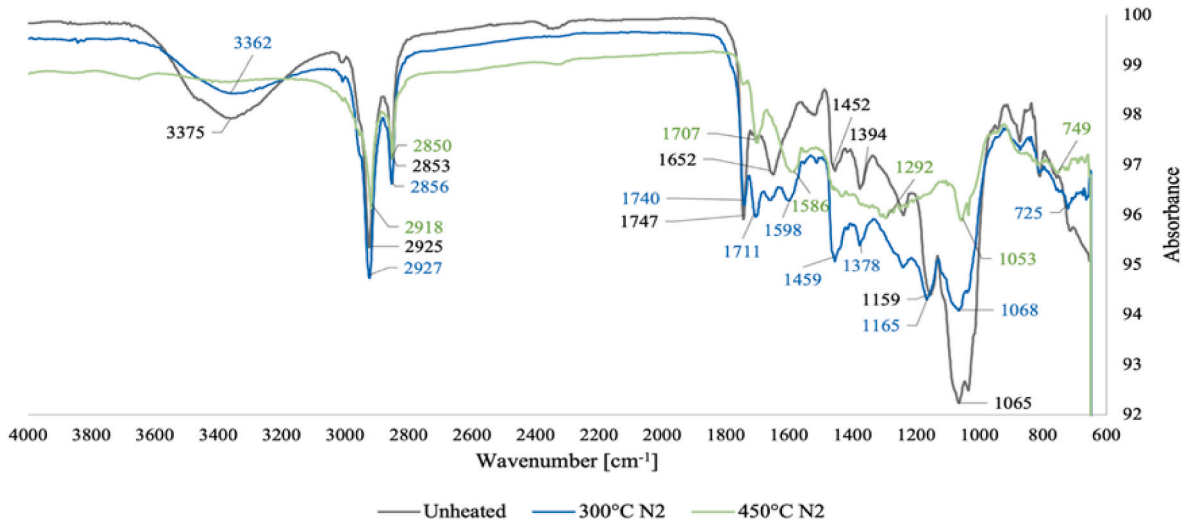


**Fig. 1.** FTIR spectra of unheated SCG in comparison with biochar type 300 °C $N_2$ and 450 °C $N_2$.

**Table 2**
EDXS analyses of unheated SCG compared to biochar type 450 °C $N_2$.

| Biochar type | | O | Mg | P | K | Ca | Cl | Al | S | Sum |
|---|---|---|---|---|---|---|---|---|---|---|
| *Unheated SCG* | Mass [%] | 89.5 | 1.4 | 1.0 | 3.0 | 1.8 | | | 3.3 | 100 |
| | σ | 0.5 | 0.3 | 0.5 | 1.7 | 0.9 | | | 0.5 | |
| *450°C $N_2$* | Mass [%] | 69.1 | 4.9 | 2.0 | 13.1 | 6.82 | 1.14 | 1.29 | 1.64 | 100 |
| | σ | 0.6 | 0.6 | 0.1 | 0.1 | 0.03 | 0.08 | 0.08 | 0.08 | |

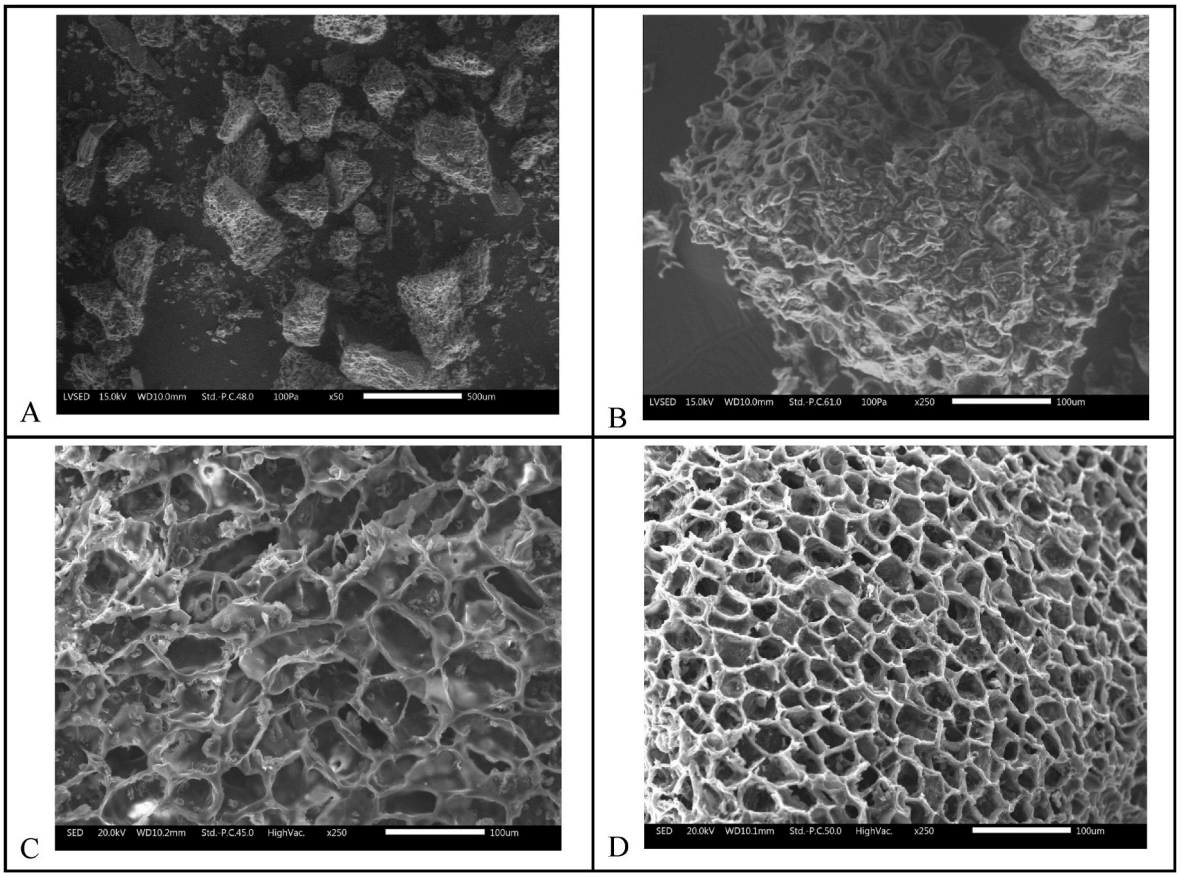


**Fig. 2.** SED images of (A) unheated SCG at magnification 50x and (B) 250x, in comparison with (C) biochar type 300 °C $N_2$ at 250x and (D) biochar type 450 °C $N_2$ at 250x.

morphology with increased porosity (Fig. 2C and D).

SCG is comprised of particles that exhibit relatively high purity and possess a uniform and well-graded structure. Srivastava (2020) investigated the particle size distribution of SCG, revealing sizes ranging from 0.1 to 2 mm, with the majority falling between 0.6 mm and 0.875 mm.

In contrast, biochar displayed a structure abundant in pores and possessing a large surface area, which provides numerous active sites for P adsorption and enhances the efficiency of the mass transfer process. The formation of this porous structure was facilitated by the rapid release of numerous volatile substances from the initial biomass structure during pyrolysis. This is supported by EDXS analysis, which reveals a decrease in oxygen (from 89.1% to 69.1%) and sulphur content (from 3.38% to 1.64%) from unheated SCG to pyrolyzed biochar (Table 2). This reduction can be attributed to the production of non-condensable gases as combustion byproducts during pyrolysis. Notably, higher pyrolysis temperatures result in a larger biochar surface area and, theoretically, a higher adsorption capacity. However, extremely high temperatures can lead to a reduction in active sites due to the collapse of the porous structure and pores obstruction. Pyrolyzed biochar (Table 2) comprises two additional elements compared to unheated biochar: aluminum and chlorine. The presence of aluminum possibly originates from contamination from aluminium pans used to hold the biochar in the early stages of production, while the presence of chlorine is consistent with the use of dichloromethane during wash procedure.

### 3.2. Characterization of Fe-activated biochar

In FTIR analysis, the spectra of biochar coated with $FeCl_3$ exhibited medium peaks at the wave number of 1351 $cm^{-1}$ (Fig. 3) attributed to the presence of O-H bending. Furthermore, medium sharp peaks around 3682 $cm^{-1}$ were displayed by the Fe-activated biochar, indicating the presence of O-H stretching. The hydroxyl group is crucial for an effective sorption by biochar and its presence demonstrates the efficacy of the functionalization method implemented by biochar impregnation with $FeCl_3$ solution.

The comparison between backscattered electron detector (BED, Fig. 4) images of non-activated and Fe-activated biochar are useful to address the chemical composition of the granules. In Fig. 4B, white dots can be observed that indicate the presence of elements with heavy atomic mass, namely iron.

Confirmation of the presence of Fe coated onto the biochar's surface was established through EDXS analysis of the biochar type 450 °C $N_2$ Fe-activated (Table 3). In this activated biochar, Fe accounted for 3.87, while Cl content was measured at 4.65%, notably elevated compared to the Cl percentage of 1.14% in the non-activated biochar type 450 °C $N_2$ (indicated in Table 2).

Conversely, there are no significant differences in the content of the other elements before and after the chemical activation (Tables 2 and 3). The presence of various metal elements, namely Fe, Mg, Ca, Al, and numerous surface functional groups is fundamental for the adsorption capacity of biochar, serving as active sites for diffusion or through the formation of mineral precipitates or surface complexation.

The impregnation capability of biochar, based on impregnation ratio and activation method, was evaluated through EDXS spectra analysis, with the resulting Fe content values reported in Table 4.

Iron content rises as the Fe/biochar ratio increases, as expected (see Table 4). Biochar produced at different pyrolysis temperatures display comparable impregnation capability when the Fe/biochar ratio is the same. Varying depth of EDXS analysis, it was observed that Fe content is higher on biochar surface and decreases as the biomass is penetrated more.

The iron values impregnated on the biomass, as reported in Table 4, do not exhibit a direct proportionality to the Fe/biochar mass ratio and the percentages remain low. The limited impregnation can be attributed to the acidic conditions formed at weight ratio of Fe/biochar greater than 1. In such acidic environments, iron binding to biochar is predominantly governed by adsorption (Anonymous Reviewer, 2024). As a result, only strongly bound Fe species effectively coat onto the biochar, while weakly adsorbed ones are possibly removed during the washing procedure following impregnation.

### 3.3. Phosphate removal from water by SCG biochar

A sequence of batch adsorption tests was conducted to evaluate the phosphate adsorption capacity of SCG biochar and establish the corresponding isotherms. Batch experiments are employed to assess variations in adsorption efficiency, typically represented by constructing plots that depict the adsorbed quantity as a function of the initial concentration. The shape of this plot provides insights into the nature of the adsorption, guiding the modeling of kinetics accordingly.

The first set of experiments was performed with an initial P concentration of 15 mg P/L. The objective was to investigate the influence

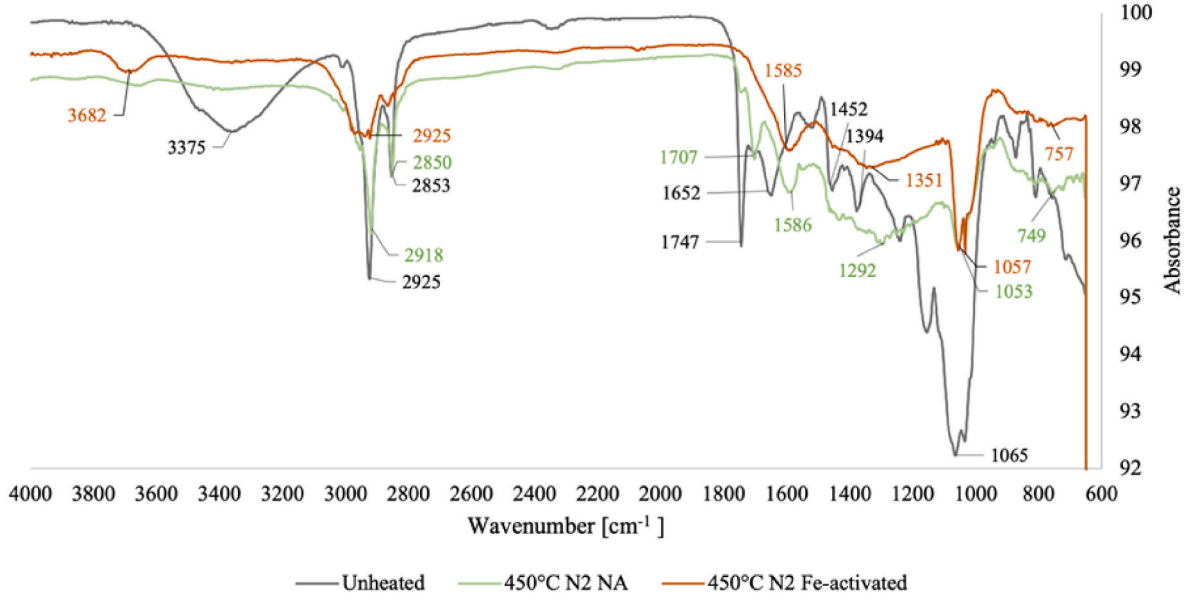


**Fig. 3.** FTIR spectra of Fe-activated biochar (450 °C $N_2$ Fe-activated) in comparison with unheated SCG and non-activated biochar type 450 °C $N_2$ NA.

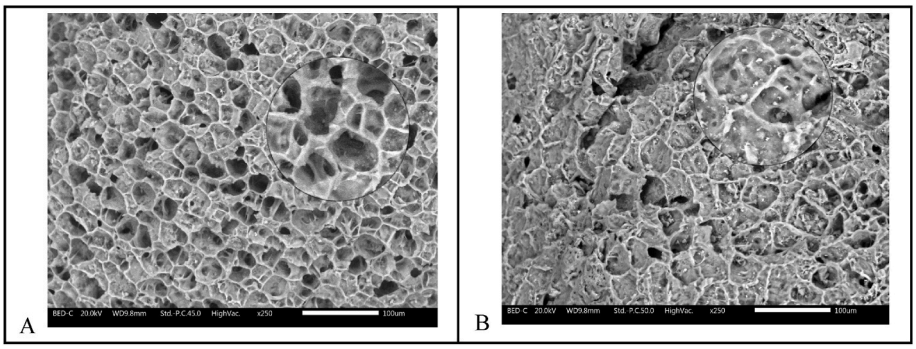


**Fig. 4.** BED images of (A) non-activated biochar type 450 °C N2 NA in comparison with (B) functionalized biochar type 450 °C $N_2$ Fe-activated.

**Table 3**
EDXS analyses of functionalized biochar type 450 °C $N_2$ Fe-activated.

| Biochar type | | O | Mg | P | K | Ca | Cl | Al | S | Fe | Sum |
|---|---|---|---|---|---|---|---|---|---|---|---|
| *450°C $N_2$* | Mass [%] | 55.8 | 5.0 | 2.3 | 19.6 | 6.5 | 4.7 | 0.5 | 1.7 | 3.9 | 100 |
| *Fe-activated* | σ | 1.5 | 1.4 | 1.3 | 4.2 | 0.1 | 0.4 | 0.3 | 0.6 | 2.1 | |

**Table 4**
EDXS analyses of Fe content across different Fe-activated biochar types.

| Biochar type | Fe/biochar | Element | Mass | | Atom | |
|---|---|---|---|---|---|---|
| | | | [%] | σ | [%] | σ |
| *450°C $N_2$* | 05:1 | Fe | 2.69 | 1.954 | 1.08 | 0.787 |
| *450°C $N_2$* | 1:1 | Fe | 2.80 | 1.211 | 1.14 | 0.516 |
| *450°C $N_2$* | 2:1 | Fe | 3.87 | 2.125 | 1.50 | 0.777 |
| *500°C $N_2$* | 2:1 | Fe | 3.02 | 0.465 | 1.13 | 0.100 |

of the following operational factors on the adsorption capacity ($q_e$): (i) the optimum heating temperature during pyrolysis, (ii) the activation level of biochar in terms of Fe/biochar mass ratio, (iii) the sorption capacity of the Fe-activated biochar in comparison with non-activated biochar. Results are shown in Fig. 5 and discussed below.

P adsorption capacity across all Fe/biochar ratios (Fig. 5A) increases with rising pyrolysis temperature beyond 300 °C, reaching its maximum at 450 °C and subsequently declining above 500 °C. One plausible explanation for this behavior is the reduction in active sites that occurs at higher temperatures, attributed to the collapse of the porous structure and obstruction of pores (Zhang et al., 2022). In addition, biochar produced at 450 °C was found to display a slightly greater amount of Fe coated on its surface (3.9% by mass), compared to biochar produced at 500° (3.0%), when the Fe/biochar ratio was the same (2:1). As shown in Fig. 5A, the higher adsorption capacity was found using the highest Fe/biochar ratio of 2:1; in this case, the values of $q_e$ were 0.58, 0.63, 0.87, 0.78 and 0.51 mg P/g at pyrolysis temperatures of 300 °C, 350 °C, 450 °C, 500 °C and 550 °C, respectively. The maximum $q_e$ (0.87 mg P/g) occurs at Fe/biochar ratio of 2:1 and pyrolysis temperature of 450 °C.

The upward trend of adsorption capacity in Fig. 5B confirms that the amount of P adsorbed by biochar activated under different Fe/biochar ratios rises as the rate of Fe increases. Chemical activation with increasing FeCl3 ratio enhances metal-ion availability for surface precipitation and complexation. As regards the biochar produced at 450 °C, the values of $q_e$ were 0.43, 0.47, 0.71 and 0.87 mg P/g at Fe/biochar ratios of 0:1, 0.5:1, 1:1 and 2:1, respectively.

The value of $q_e$ of non-activated biochar produced at 450 °C (Fig. 5A) was 0.43 mg P/g, comparable with $q_e$ of 0.47 mg P/g obtained using biochar at Fe/biochar ratio of 0.5:1, which is an indication that the amount of Fe coated was not enough to achieve removal efficiencies significantly greater than that of untreated biochar. Instead, when biochar produced at 450 °C was activated with Fe/biochar ratio of 2:1, $q_e$ doubled from 0.43 to 0.87 mg P/g, proving that the major adsorption sites of the biomass were provided by metal oxides coated onto its surface.

Overall, the results of the adsorption batch tests confirmed that $q_e$ of

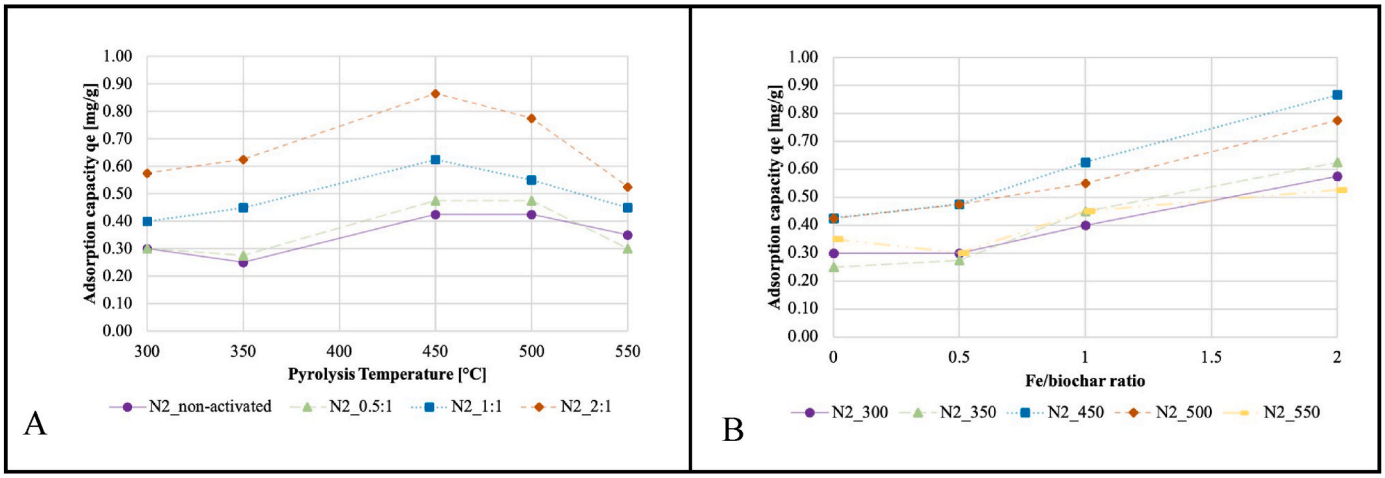


**Fig. 5.** Equilibrium adsorption capacity of Fe-activated and non-activated biochar as a function of (A) pyrolysis temperature and (B) Fe/biochar mass ratio.

biochar was influenced by the pyrolysis temperature and activation conditions of the adsorbent. The introduction of ferric chloride effectively improved $q_e$, through the formation of phosphate-iron complexes due to the functionalization, that is the enhancement of the surface functional groups and surface area of the adsorbent. However, the amount of P adsorbed by SCG biochar appears to be relatively low, even for activated SCG biochar. Findings align with reported P removal efficiency values of non-activated wheat straw biochar (approximately 5.3%) reported by Li et al., (2014). The iron coated on SCG biochar, constituting around 3% by mass, is notably lower than the range of 25% and 65% reported in Li and coworkers' research for activated wheat straw biochar. This discrepancy may account for the considerable difference in total P adsorption between activated wheat straw biochar and activated SCG biochar. The observed low phosphorus adsorption capacity may be reasonably explained by the biochar surface's inherent negative charge, causing electrostatic repulsion with negatively charged ions like phosphate. Additionally, it has been demonstrated that different iron oxides possess varying adsorption capacities for phosphate, which can be attributed to differences in manufacturing temperatures and production processes. This variability may arise from the diverse crystalline phases and locations of Fe oxides, whether on the surface or embedded within biochar (Zhao et al., 2006). During pre-pyrolysis activation, activating agents are introduced onto the biomass, facilitating the formation of complexes on the surfaces of the resulting biochar. Conversely, in post-pyrolysis activation, these agents are directly applied to the biochar, enabling the creation of new adsorption sites but potentially resulting in lower activation effectiveness (Pathy et al., 2023).

Although the post-pyrolysis chemical treatment with FeCl3 adopted in this study effectively generates more positive sites on the biochar surface, thereby enhancing $q_e$ values, the limited amount of Fe coated on the SCG biochar may remain the limiting factor for achieving high P removal efficiencies.

### 3.4. Adsorption isotherms of P on Fe-activated and non-activated biochar

Batch experiments were carried out in parallel with increasing concentrations of initial P (2, 5, 10 mg P/L) and using 2.0 g/L of the following types of adsorbents: (1) activated biochar 450 °C $N_2$ with Fe/biochar ratio of 2:1, which gave the highest adsorption capability $q_e$ (see section 3.4), (2) non-activated biochar type 450 °C $N_2$ NA. At the end of the adsorption tests, the equilibrium concentration of P in the solution ($C_e$) was analyzed and used for the calculation of the isotherms. The comparison between the adsorption isotherms equations, parameters and constants is summarized in Table 5.

For both biochar, higher $q_e$ values were observed when the initial P concentration in the solution was the highest (15 mg P/L). At an initial P concentration of 15 mg P/L, the activated biochar 450 °C $N_2$ 2:1 exhibited a $q_e$ value of 0.87 mg P/g, corresponding to a removal efficiency of 11.5%. In comparison, the non-activated biochar type 450 °C $N_2$ NA showed a $q_e$ value of 0.43 mg P/g, with a corresponding removal efficiency of 5.7%.

In contrast, the highest removal efficiencies for phosphorus were achieved at the lowest initial concentrations, reaching 13.8% and 17.3% (in relation to 450 °C $N_2$ activated biochar) when the initial P concentrations in the solution were 2.0 mg/L and 5.0 mg/L, respectively. This is possibly due to an increased resistance in the diffusion of the adsorbate onto the adsorbents' surfaces and saturation of active sites at higher concentrations. The polynomial regression equations for determining the amount of P adsorbed are $y = 0.056x + 0.0984$ ($R^2 = 0.9296$) for 450 °C $N_2$ 2:1 SCG biochar and $y = 0.0277x + 0.0038$ ($R^2 = 0.9193$) for 450 °C $N_2$ non-activated SCG biochar. The P adsorption behavior of activated and non-activated biochar was then addressed using the Langmuir and Freundlich isotherms expressed as linear form. Mathematical models' parameters were estimated using linear regression.

Langmuir dimensionless equilibrium parameter RL, calculated as mean value for each different initial concentration, was found to be between 0 and 1, indicating favorable adsorption process. The same conclusion can be drawn from Freundlich n values of the both biochar: values between 1 and 10 generally indicates that biochar is conducive to phosphorus removal.

The Langmuir adsorption equilibrium constant (b), related to the binding strength of the adsorbate, was 0.110 for activated biochar type 450 °C $N_2$ and 0.071 for non-activated biochar 450 °C $N_2$. The b value shown by activated biochar is thus 1.56 times higher than that of raw biochar without FeCl3 chemical activation. Higher values of the binding strength constant b have been related to specific adsorption of phosphate at high-energy surfaces with low dissociation constants (Park et al., 2015). On the other hand, lower b values are demonstrated to be related to sorption at low-energy surfaces with high dissociation constants (Park et al., 2015).

Greater Freundlich n and Kf values entail higher P sorption capabilities: the adsorption capacity of 450 °C $N_2$ activated biochar was found to be greater than that of biochar prepared without FeCl3. However, Freundlich exponent 1/n being close to 1, entails that the saturation point was not reached. The Freundlich model gave the higher $R^2$ values, meaning that the equilibrium adsorption data fitted the Freundlich mathematical model significantly better. From these results it can be inferred that phosphorus adsorption on SCG biochar is governed by heterogeneous processes. Indeed, the Freundlich model is commonly employed to evaluate chemisorption on heterogeneous surfaces characterized by a non-uniform distribution of active sites and their energies across the surface (Park et al., 2015).

### 3.5. P desorption from biochar

Phosphate desorbability was investigated to evaluate the stability of biochar, as it can affect the bioavailability of nutrients onto biochar-enriched composites and their potential to be reused as fertilizer for soil enhancement. Phosphate desorbability is defined as the ratio of the P desorbed to the total P adsorbed by the biomass, and it represents a suitable index to assess the degree of phosphate desorption from the adsorbent (Trazzi et al., 2016).

The control desorption tests conducted with biochar that had not undergone adsorption batch experiments, showed that no significant amount of P was released from biochar prior to P-adsorption. Results of desorption experiments from biochar prior to adsorption and P-adsorbed biochar produced at different pyrolysis temperatures and activated under different conditions, are reported as mean values (Table 6).

Mean value of P desorbability of the samples that underwent desorption experiment was 52%, consistently with P release values found by Trazzi et al. (2016), whose study elucidated that the rate of

**Table 5**
Langmuir and Freundlich isotherm parameters and constants for the adsorption of P on activated biochar type 450 °C $N_2$ 2:1 and non-activated 450 °C $N_2$ NA biochar.

| Biochar type | Langmuir | | | | Freundlich | | | |
|---|---|---|---|---|---|---|---|---|
| | $R^2$ | $q_0$ [mg/g] | b [L/mg] | $R_L$ | $R^2$ | 1/n | $K_f$ [mg/g] | n |
| *450°C $N_2$ Fe/biochar 2:1* | 0.504 | 0.87 | 0.110 | 0.579 | 0.934 | 0.833 | 0.340 | 1.200 |
| | Equation y = 0.442x + 10.432 | | | | Equation y = 0.833x + 1.000 | | | |
| *450°C $N_2$ NA* | 0.106 | 0.43 | 0.071 | 0.671 | 0.952 | 0.892 | 0.230 | 1.115 |
| | Equation y = 0.485 x + 32.899 | | | | Equation y = 0.892 x + 1.473 | | | |

**Table 6**
Mean values of P desorbed from biochar prior to adsorption and from non-activated and Fe-activated P-adsorbed biochar.

| Biochar type | Fe/ biochar | $C_0$ | P adsorbed [mg/g] | P desorbed [mg/g] | Desorbability [%] |
|---|---|---|---|---|---|
| *450°C $N_2$* | NA | – | – | 0.09 | – |
| *450°C $N_2$* | 2:1 | – | – | 0.05 | – |
| *500°C $N_2$* | 2:1 | – | – | 0.03 | – |
| *350°C $N_2$* | NA | 15.0 | 0.85 | 0.34 | 39.4 |
| *450°C $N_2$* | NA | 15.0 | 0.50 | 0.15 | 29.0 |
| *500°C $N_2$* | NA | 15.0 | 0.80 | 0.34 | 42.5 |
| *450°C $N_2$* | 2:1 | 2.0 | 0.49 | 0.23 | 46.9 |
| *450°C $N_2$* | 2:1 | 10.0 | 0.33 | 0.24 | 72.7 |
| *500°C $N_2$* | 2:1 | 15.0 | 0.60 | 0.37 | 61.7 |

phosphate desorption from biochar is highly dependent on the gradient of phosphate adsorbed and the concentrations of various ions in solution.

While the amount of P previously adsorbed by SCG biochar may appear relatively low, the effectiveness of P desorption from P-adsorbed biochar within 4 h of testing proved to be significant compared to raw SCG biochar. During desorption experiments with P-adsorbed biochar, phosphate salts – observed as insoluble particles - were released into the solution, indicating that P-adsorbed biochar presents an appropriate rate of P release. This characteristic is crucial in agricultural soils for practical application.

Specifically, Fe-activated biochar exhibited a higher phosphorus release rate (60%) compared to non-activated biochar (37%). Once again, the biochar modification step proves necessary to improve the P absorption and desorption capabilities of biochar. The resultant biochar, enriched with Fe-phosphate, can be recovered and potentially reused for soil remediation, contributing to increased soil fertility and enhanced crop productivity.

## 4. Conclusions

Spent coffee grounds demonstrated significant promise as a biomass to produce biochar, with yields ranging from 25% to 64% depending on the pyrolysis temperature within the 300–550 °C range. P adsorption capability of SCG biochar was found to be influenced by the pyrolysis temperature and activation conditions, as well as initial P concentration, in agreement with previous studies on biochar produced from Miscanthus Giganteus (Trazzi et al., 2016), wheat straw (Li et al., 2014), sesame straw (Park et al., 2015). FTIR analysis conducted on both unheated, pyrolyzed and activated biochar samples indicated the presence of C-H, C=O and O-H functional groups on the biochar surface. As the pyrolysis temperature rises, the total number of functional groups decrease. Notably, biochar activated with FeCl3 exhibited the presence of the hydroxyl group, which was absent in the FTIR spectra of non-activated SCG pyrolyzed at temperatures greater than 300 °C. This demonstrates that the functional groups of biochar can be functionalized to accommodate iron salts and, due to their high affinity with phosphate, this results in an enhanced adsorption capacity of P by Fe-activated biochar.

SCG biochar exhibited an upward trend of adsorption capacity when the pyrolysis temperature and/or the Fe/biochar mass ratio increased, confirming that the heating process and chemical activation contribute to a greater availability of active sites for adsorption. Nonetheless, the limited amount of Fe coated on the SCG biochar remains a significant limitation in achieving optimal P removal efficiencies. The low Fe content values are attributed to the impregnation procedure adopted in this study, which occurred post-pyrolysis. While this approach offers the advantage of adaptability to pre-existing biochar, it results in a restricted Fe impregnation. This limitation underlines the need for further optimization of activation techniques to enhance the effectiveness of SCG biochar in P recovery applications.

## CRediT authorship contribution statement

**Alessia Torboli:** Writing – original draft, Methodology, Investigation, Formal analysis, Conceptualization. **Paola Foladori:** Writing – review & editing, Project administration, Methodology, Conceptualization. **Mingming Lu:** Writing – review & editing, Project administration, Methodology, Conceptualization. **Stefano Gialanella:** Writing – review & editing, Validation, Conceptualization. **Lorena Maines:** Writing – review & editing, Methodology, Formal analysis.

## Declaration of competing interest

The authors declare that they have no known competing financial interests or personal relationships that could have appeared to influence the work reported in this paper.

## Acknowledgements

We acknowledge the support from the College of Engineering & Applied Science (University of Cincinnati). This study was funded partially by the US National Science Foundation (grant #1919114).

We thank the anonymous reviewers for their thoughtful comments and efforts towards significantly improving the quality of our manuscript.

## Data availability

Data will be made available on request.

## References

Ahmad, M., Rajapaksha, A.U., Lim, J.E., Zhang, M., Bolan, N., Mohan, D., Vithanage, M., Lee, S.S., Ok, Y.S., 2014. Biochar as a sorbent for contaminant management in soil and water: a review. Chemosphere 99, 19–33. https://doi.org/10.1016/j.chemosphere.2013.10.071.

Ahmed, H., Abolore, R.S., Jaiswal, S., Jaiswal, A.K., 2024. Toward circular economy: potentials of spent coffee grounds in bioproducts and chemical production. Biomass 4 (2), 286–312. https://doi.org/10.3390/biomass4020014.

Anonymous Reviewer, 2024. Comments to the Original Manuscript Submitted to Cleaner Engineering and Technology.

Ajmal, Z., Muhmood, A., Dong, R., Wu, S., 2020. Probing the efficiency of magnetically modified biomass-derived biochar for effective phosphate removal. J. Environ. Manag. 253, 109730. https://doi.org/10.1016/j.jenvman.2019.109730.

Chen, B., Zhou, D., Zhu, L., 2008. Transitional adsorption and partition of nonpolar and polar aromatic contaminants by biochars of pine needles with different pyrolytic temperatures. Environ. Sci. Technol. 42, 5137–5143. https://doi.org/10.1021/es8002684.

Cordell, D., Neset, T.-S.S., Prior, T., 2012. The phosphorus mass balance: identifying "hotspots" in the food system as a roadmap to phosphorus security. Curr. Opin. Biotechnol. 23, 839–845. https://doi.org/10.1016/j.copbio.2012.03.010.

De Bomfim, A.S.C., De Oliveira, D.M., Walling, E., Babin, A., Hersant, G., Vaneeckhaute, C., Rodrigue, D., 2023. Spent coffee grounds characterization and reuse in composting and soil amendment. Waste 1, 2–20.

Fang, C., Zhang, T., Li, P., Jiang, R., Wu, S., Nie, H., Wang, Y., 2015. Phosphorus recovery from biogas fermentation liquid by Ca-Mg loaded biochar. J. Environ. Sci. (China) 29, 106–114. https://doi.org/10.1016/j.jes.2014.08.019.

Guo, M., Song, W., Tian, J., 2020. Biochar-facilitated soil remediation: mechanisms and efficacy variations. Front. Environ. Sci. 8, 521512. https://doi.org/10.3389/fenvs.2020.521512.

Gwenzi, W., Chaukura, N., Noubactep, C., Mukome, F.N.D., 2017. Biochar-based water treatment systems as a potential low-cost and sustainable technology for clean water provision. J. Environ. Manag. 197, 732–749. https://doi.org/10.1016/j.jenvman.2017.03.087.

Harvey, O.R., Herbert, B.E., Kuo, L.-J., Louchouarn, P., 2012. Generalized two-dimensional perturbation correlation infrared spectroscopy reveals mechanisms for the development of surface charge and recalcitrance in plant-derived biochars. Environ. Sci. Technol. 46, 10641–10650. https://doi.org/10.1021/es302971d.

Johnson, K., Liu, Y., Lu, M., 2022. A review of recent advances in spent coffee grounds upcycle technologies and practices. Front. Chem. Eng. 4. https://doi.org/10.3389/fceng.2022.838605.

Kopecký, M., Kolář, L., Konvalina, P., Strunecký, O., Teodorescu, F., Mráz, P., Peterka, J., Váchalová, R., Bernas, J., Bartoš, P., Filipov, F., Bucur, D., 2020. Modified biochar—a tool for wastewater treatment. Energies 13 (20), 5270. https://doi.org/10.3390/en13205270.

Li, J.-H., Lv, G.-H., Bai, W.-B., Liu, Q., Zhang, Y.-C., 2014. Modification and use of biochar from wheat straw (Triticum aestivum L.) for nitrate and phosphate removal from water. Desalination Water Treat. 56, 4681–4693.

Lichtenberg, H., Prange, A., Modrow, H., Hormes, J., 2007. Characterization of sulfur compounds in coffee beans by sulfur K-XANES spectroscopy. In: AIP Conference Proceedings. Presented at the X-RAY ABSORPTION FINE STRUCTURE - XAFS13: 13th International Conference. AIP. https://doi.org/10.1063/1.2644676.

Lu, M., Liu, J., Zhou, Y., Srivastava, S., Xu, D., Williams, E., Schwein, G., 2020. Spent coffee ground (SCG) biochar for select heavy metal removal. A&WMA's 113th Annual Conference & Exhibition. San Francisco, California.

Luo, D., Wang, L., Nan, H., Cao, Y., Wang, H., Kumar, T.V., Wang, C., 2023. Phosphorus adsorption by functionalized biochar: a review. Environ. Chem. Lett. 21 (1), 497–524. https://doi.org/10.1007/s10311-022-01519-5.

Nardis, B.O., Franca, J.R., Carneiro, J.S.D.S., Soares, J.R., Guilherme, L.R.G., Silva, C.A., Melo, L.C.A., 2022. Production of engineered-biochar under different pyrolysis conditions for phosphorus removal from aqueous solution. Sci. Total Environ. 816, 151559. https://doi.org/10.1016/j.scitotenv.2021.151559.

Nassef, E., 2012. Removal of phosphates from industrial waste water by chemical precipitation, engineering science and technology. Int. J. 2, 2250–3498.

Nguyen, V.-T., Nguyen, T.-B., Chen, C.-W., Hung, C.-M., Vo, T.-D.-H., Chang, J.-H., Dong, C.-D., 2019. Influence of pyrolysis temperature on polycyclic aromatic hydrocarbons production and tetracycline adsorption behavior of biochar derived from spent coffee ground. Bioresour. Technol. 284, 197–203. https://doi.org/10.1016/j.biortech.2019.03.096.

Park, J.H., Ok, Y.S., Kim, S.H., Cho, J.S., Heo, J.S., Delaune, R.D., Seo, D.C., 2015. Evaluation of phosphorus adsorption capacity of sesame straw biochar on aqueous solution: influence of activation methods and pyrolysis temperatures. Environ. Geochem. Health 37, 969–983. https://doi.org/10.1007/s10653-015-9709-9.

Pathy, A., Pokharel, P., Chen, X., Balasubramanian, P., Chang, S.X., 2023. Activation methods increase biochar's potential for heavy-metal adsorption and environmental remediation: a global meta-analysis. Sci. Total Environ. 865, 161252. https://doi.org/10.1016/j.scitotenv.2022.161252.

Pivokonský, M., Novotná, K., Čermáková, L., Petříček, R., 2022. Jar Tests for Water Treatment Optimisation: How to Perform Jar Tests – a Handbook. IWA Publishing. https://doi.org/10.2166/9781789062694.

Rizwan, M., Murtaza, G., Zulfiqar, F., Moosa, A., Iqbal, R., Ahmed, Z., Irshad, S., Khan, I., Li, T., Chen, J., Zhang, M., Siddique, K.H.M., Leng, L., Li, H., 2023. Sustainable manufacture and application of biochar to improve soil properties and remediate soil contaminated with organic impurities: a systematic review. Front. Environ. Sci. 11, 1277240. https://doi.org/10.3389/fenvs.2023.1277240.

Sahoo, S.S., Vijay, V.K., Chandra, R., Kumar, H., 2021. Production and characterization of biochar produced from slow pyrolysis of pigeon pea stalk and bamboo. Clean. Eng. Technol. 3, 100101. https://doi.org/10.1016/j.clet.2021.100101.

Schröder, J., Cordell, D., Smit, A., Rosemarin, A., 2010. Sustainable Use of Phosphorus, Waganingen UR, The Netherlands. Report 357.

Sharma, T., Hakeem, I.G., Gupta, A.B., Joshi, J., Shah, K., Vuppaladadiyam, A.K., Sharma, A., 2024. Parametric influence of process conditions on thermochemical techniques for biochar production: a state-of-the-art review. J. Energy Inst. 113, 101559. https://doi.org/10.1016/j.joei.2024.101559.

Sheperd, J., Sohi, S., Heal, K., 2016. Optimising the recovery and re-use of phosphorus from wastewater effluent for sustainable fertiliser development. Water Res. 94, 155–165..

Srivastava, S., 2020. Zero Waste Utilization of the Spent Coffee Ground by Extracting the Coffee Biodiesel and Converting Left over Remains into the Biochar for Heavy Metal Pollutant Removal from the Aqueous Medium.

Tan, I.A.W., Hameed, B.H., Ahmad, A.L., 2007. Equilibrium and kinetic studies on basic dye adsorption by oil palm fibre activated carbon. Chem. Eng. J. 127, 111–119. https://doi.org/10.1016/j.cej.2006.09.010.

Tomczyk, A., Sokołowska, Z., Boguta, P., 2020. Biochar physicochemical properties: pyrolysis temperature and feedstock kind effects. Rev. Environ. Sci. Biotechnol. 19 (1), 191–215. https://doi.org/10.1007/s11157-020-09523-3.

Trazzi, P.A., Leahy, J.J., Hayes, M.H.B., Kwapinski, W., 2016. Adsorption and desorption of phosphate on biochars. J. Environ. Chem. Eng. 4, 37–46. https://doi.org/10.1016/j.jece.2015.11.005.

Wang, C., Wang, Y., Herath, H.M.S.K., 2017. Polycyclic aromatic hydrocarbons (PAHs) in biochar – their formation, occurrence and analysis: a review. Org. Geochem. 114, 1–11. https://doi.org/10.1016/j.orggeochem.2017.09.001.

Xiao, X., Chen, Z., Chen, B., 2016. H/C atomic ratio as a smart linkage between pyrolytic temperatures, aromatic clusters and sorption properties of biochars derived from diverse precursory materials. Sci. Rep. 6, 22644. https://doi.org/10.1038/srep22644.

Yin, Q., Liu, M., Ren, H., 2019. Biochar produced from the co-pyrolysis of sewage sludge and walnut shell for ammonium and phosphate adsorption from water. J. Environ. Manag. 249, 109410. https://doi.org/10.1016/j.jenvman.2019.109410.

Zhang, X., Zhao, B., Liu, H., Zhao, Y., Li, L., 2022. Effects of pyrolysis temperature on biochar's characteristics and speciation and environmental risks of heavy metals in sewage sludge biochars. Environ. Technol. Innovat. 26, 102288. https://doi.org/10.1016/j.eti.2022.102288.

Zhao, L., Yang, H., Li, S., Yu, L., Cui, Y., Zhao, X., Feng, S., 2006. The effect of aging time and calcination temperature on the magnetic properties of α-Fe/Fe3O4 composite. J. Magn. Magn Mater. 301 (2), 287–291. https://doi.org/10.1016/j.jmmm.2005.07.029.